Superparamagnetic Hollow and Paramagnetic Porous Gd_2O_3 Particles

Chih-Chia Huang,[†,‡] Tzu-Yu Liu,[†,‡] Chia-Hao Su,[§] Yi-Wei Lo,[‡] Jyh-Horng Chen,[§] and Chen-Sheng Yeh*[,‡]

Department of Chemistry, National Cheng Kung University, Tainan 701, Taiwan, and Department of Electrical Engineering, National Taiwan University, Taipei 106, Taiwan

Received November 9, 2007. Revised Manuscript Received April 9, 2008

We have successfully introduced biological gelatin particles as center cores acting as shape and structure directors to form superparamagnetic hollow and paramagnetic porous Gd_2O_3 particles, which have average sizes below 200 nm. Two approaches involving sol−gel processes and precursor deposition induced by solvent evaporation were employed to fabricate hollow and porous particles, respectively. The magnetization measurements including ZFC-FC curves and magnetization vs *H/T* as well as their usefulness for in vitro MR imaging were investigated for Gd_2O_3 particles. With the presence of carbon residue on the hollow Gd_2O_3 surface, the hollow Gd_2O_3 particles exhibited superparamagnetic behavior. However, these hollow species turned paramagnetic after removal of the carbon-based residue. The hollow and porous Gd_2O_3 nanospheres all indicated satisfactory biocompatibility from the measurements of the leaching behavior of Gd^{3+} ions and cell culture viability. We found, from positive contrast images in in vitro MR assays, that they are capable of providing high-contrast MR images. Furthermore, this synthetic strategy using biological gelatin particles as templates could be readily extended to form TiO_2 (porous and hollow) particles.

Introduction

The magnetic resonance (MR) effect discovered in the 1920s is based on the magnetic properties of hydrogen nuclei. The protons produce the net magnetic moment under an external magnetic field. It has been recognized as one of the important techniques in medical diagnosis. For MR imaging, an accurate diagnosis is obtained by using positive contrast agents, such as ionic gadolinium (Gd)-based[1] and Mn-based[2] materials, or negative contrast agents,[3,4] such as superparamagnetic iron oxide (SPIO) and ultrasmall SPIO (USPIO)[4], to enhance the contrast of images in living tissue.[1] Recently, we presented Au_3Cu_1 nanoshells with bimodal MR contrast agents for T_1 and T_2 contrast enhancement[5] and T_2 negative iron oxide nanoparticles[4] for an in vitro assay and an in vivo animal model. Porous Au_3Cu_1 nanoshells with a high surface area are likely to be adsorbent and allow a large amount of water interpenetration and favor water coordination to poly surface sites of the materials. Therefore, the porous nanoshell provides better contrast in MR imaging.[5] Additionally, hollow and porous structures have enormous potential for drug storage and delivery.[5–8] Hence, we fabricated MR-related contrast nanomaterials with hollow and porous structures.

Because of a large number of unpaired electrons in the gadolinium ion, complex species of Gd^{3+}ion have been commonly used as an MR contrast agent for positive-intensity images.[1] Recently, Gd_2O_3 nanoparticles promised and demonstrated a positive contrast effect for T_1-weighted imaging.[9] They displayed the potential applications combining with fluorescence to achieve multiimaging in vivo.[9b] A variety of hollow and porous materials have been fabricated. However, the hollow and porous Gd_2O_3 particles

* Corresponding author. E-mail: csyeh@mail.ncku.edu.tw.
† National Cheng Kung University.
‡ C.-C.H. and T.-Y.L. contributed equally to this article.
§ National Taiwan University.

(1) (a) Endres, P. J.; Paunesku, T.; Vogt, S.; Meade, T. J.; Woloschak, G. E. *J. Am. Chem. Soc.* **2007**, *129*, 15760. (b) Kim, J. S.; Rieter, W. J.; Taylor, K. M. L.; An, H.; Lin, W.; Lin, W. *J. Am. Chem. Soc.* **2007**, *129*, 8962. (c) Caravan, P.; Ellison, J. J.; McMurry, T. J.; Lauffer, R. B. *Chem. Rev.* **1999**, *99*, 2293. (d) Mrbach, A.; Toth, E. *The Chemistry of Contrast Agents in Medical Magnetic Resonance Imaging*; John, Wiley & Sons: New York, 2001.

(2) (a) Wang, S.; Jarrett, B. R.; Kauzlarich, S. M.; Louie, A. Y. *J. Am. Chem. Soc.* **2007**, *129*, 3848. (b) Na, H. B.; Lee, J. H.; An, K.; Park, Y. I.; Park, M.; Lee, I. S.; Nam, D.-H.; Kim, S. T.; Kim, S.-H.; Kim, S.-W.; Lim, K.-H.; Kim, K.-S.; Kim, S.-O.; Hyeon, T. *Angew. Chem., Int. Ed.* **2007**, *46*, 5397. (c) Natanzon, A.; Aletras, A. H.; Hus, L. Y.; Arai, A. E. *Radiology* **2005**, *236*, 859.

(3) (a) Miyawaki, J.; Yudasaka, M.; Imai, H.; Yorimitsu, H.; Isobe, H.; Nakamura, E.; Iijima, S. *Adv. Mater.* **2006**, *18*, 1010. (b) Lee, J.-H. H.; Jun, Y.-W.; Yeon, S.-I.; Shin, J.-S.; Cheon, J. *Angew. Chem., Int. Ed.* **2006**, *45*, 8160. (c) Jun, Y.-W.; Huh, Y.-M.; Choi, J.-S.; Lee, J.-H.; Song, H.-T.; Kim, S.; Yoon, S.; Kim, K.-S.; Shin, J.-S.; Suh, J.-S.; Cheon, J. *J. Am. Chem. Soc.* **2005**, *127*, 5732. (d) Wang, Y.-X. J.; Hussain, S. M.; Krestin, G. P. *Eur. Radiol.* **2001**, *11*, 2319.

(4) (a) Kaittanis, C.; Naser, S. A.; Perez, J. M. *Nano. Lett.* **2007**, *7*, 380. (b) Hu, F.; Wei, L.; Zhou, Z.; Ran, Y.; Li, Z.; Gao, M. *Adv. Mater.* **2006**, *18*, 2553. (c) Chng, F.-Y.; Su, C.-H.; Yang, Y.-S.; Yh, C.-S.; Tasi, C.-Y.; Wu, C.-L.; Wu, M.-T.; Sheieh, D.-B. *Biomaterials* **2005**, *26*, 729. (d) Jun, L.; Shihe, Y.; Ng, K.-M.; Su, C.-H.; Yeh, C.-S.; Wu, Y.-N.; Shieh, D.-B. *Nanotechnology* **2006**, *17*, 5812.

(5) So, C.-H.; Sheu, H.-S.; Lim, C.-Y.; Huang, C.-C.; Lo, Y.-W.; Pu, Y.-C.; Weng, J.-C.; Shieh, D.-B.; Chen, J.-H.; Yeh, C.-S. *J. Am. Chem. Soc.* **2007**, *129*, 2139.

(6) Wu, P.-C.; Wang, W.-S.; Huang, Y.-T.; Shen, H.-S.; Lo, Y.-W.; Tsai, T.-L.; Shieh, D.-B.; Yeh, C.-S. *Chem. Eur. J.* **2007**, *13*, 3878.

(7) (a) Cai, Y.; Pan, H.; Xu, X.; Hu, Q.; Li, L.; Tang, R. *Chem. Mater.* **2007**, *19*, 3081. (b) Shchukin, D. G.; Sukhorukov, G. B.; Mohwald, H. *Angew. Chem., Int. Ed.* **2003**, *42*, 4471.

(8) Lin, Y.-S.; Hung, Y.; Su, J.-K.; Le, R.; Chang, C.; Lin, M.-L.; Mou, C.-Y. *J. Phys. Chem. B.* **2004**, *108*, 15608.

10.1021/cm703195u CCC: $40.75
Published on Web 05/17/2008

have not been studied yet. To the best of our knowledge, we wish to present the first report of using gelatin as a template to create superparamagnetic hollow and paramagnetic mesoporous Gd_2O_3 spheres. We investigated their magnetic properties and their usefulness for in vitro MR imaging. We found, from positive contrast images in in vitro MR assays, that they are capable of providing high contrast MR images.

Template-assisted approaches facilitate the preparation of hollow and porous nanomaterials. Despite their diversity, existing templates can be categorized into soft and hard templates. Typically, soft templates consist of vesicles, emulsions, micelles, liquid droplets, block copolymer, resins, polymer latexes, and biological matter,[10–14] while the hard templates include silica, carbon spheres, and metallic colloids.[15–17] Materials with hollow and porous nanostructures are potentially low density and have a large specific area and surface permeability that are sensitive and favorable for biological applications.[5,7,11a,15b] Additionally, hollow spheres are widely used as controlled-release capsules for drugs, dyes, cosmetics, artificial cells, and catalysts. In the case of general templates, subsequent treatments using calcination or wet-chemistry etching were selectively conducted to remove the solid core and left the frameworks consisting of inorganic species in which structures and shapes depended on the architecture of the as-formed precursor−template composite.[7b,10–17] The soft templates used for biological materials[11] are generally expensive and difficult to scale up. For example, using bacteria, DNA, or viruses as a core requires complicated purification and extraction unfavorable for synthesizing hollow and porous nanomaterials on an industrial scale. Furthermore, the soft templates usually encounter templating sphere deformation and are unstable during the reaction, resulting in the loss of their spherical shapes. In this study, we have successfully introduced biological gelatin particles as center cores acting as shape and structure directors to form hollow and porous nanospheres through sol−gel or precursor deposition induced by solvent evaporation processes (Scheme 1).

Scheme 1. Synthesis of Hollow and Porous Inorganic Nanospheres

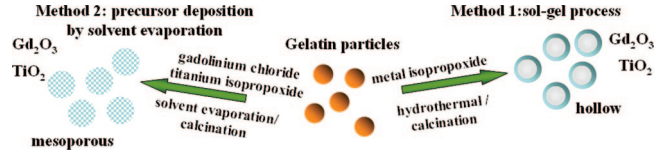

Gelatin is a protein composed of polypeptides and produced by partially hydrolyzing collagen extracted from the connective tissue of animals. It is highly soluble in water at mild temperatures. Gelatin is also a multifunctional candidate for cell culture scaffolds[18] as well as for a drug delivery carrier.[19] Using gelatin molecules as the template could be easily conducted because the surface of gelatin is rich in carboxyl and amine groups as compared with time-consuming surface modifications like polystyrene latex using layer-by-layer and acid-assisted sulfonation.[14] Using gelatin as template, we were able to form Gd_2O_3 (hollow and porous) and extended this strategy to form TiO_2 (porous and hollow) nanospheres.

Experimental Section

Materials. All reagents were of analytical purity and were used without further purification. Gelatin (Acros), $GdCl_3 \cdot 6H_2O$ (Alfa), gadolinium isopropoxide (5% in toluene/isopropyl alcohol [3:2], Alfa Aesar), and titanium isopropoxide (Acros) were purchased as organic and inorganic sources. Polyethylene oxide−polypropylene oxide−polyethylene oxide (PEO-PPO-PEO, P123) is a triblock copolymer purchased from Aldrich. The solvents toluene and isopropyl alcohol (C_3H_5OH) were purchased from Mallinckrodt, and ethanol was purchased from J. T. Backer. A 4.5 M HCl aqueous solution was prepared by diluting concentrated HCl (31.5−38%, J. T. Backer).

Preparing Gelatin Templates and as-Synthesized Nanospheres. We prepared the template reagents before preparing the hollow and porous nanospheres. We first dissolved 1.5 g of gelatin

(9) (a) Fortin, M. A.; Petoral, R. M. P., Jr.; Söderlind, F.; Klasson, A.; Engström, M.; Veres, T.; Käll, P.-O.; Uvdal, K. *Nanotechnology* **2007**, *18*, 395501. (b) Bridot, J.-L.; Faure, A.-C.; Laurent, S.; Riviere, C.; Billotey, C.; Hiba, B.; Janier, M.; Josserand, V.; Coll, J.-L. *J. Am. Chem. Soc.* **2007**, *129*, 5076. (c) McDonald, M. A.; Watkin, K. L. *Acad. Radiol.* **2006**, *13*, 421. (d) Engstrom, M.; Klasson, A.; Pedrsen, H.; Vahlberg, C.; Kall, P. O.; Uvdal, K. *Magn. Reson, Mater. Phys.* **2006**, *19*, 180. (e) McDonald, M. A.; Watkin, K. L. *Invest. Radiol.* **2003**, *38*, 305.
(10) (a) Schacht, S.; Huo, Q.; Voigt-Martin, I. G.; Stucky, G. D.; Schuth, F. *Science* **1996**, *273*, 768. (b) Djojoputri, H.; Zhou, X. F.; Qiaok, S. Z.; Wang, L. Z.; Yu, C. Z.; Lu, G. Q. *J. Am. Chem. Soc.* **2006**, *128*, 5320. (c) Rathod, S. B.; Ward, T. L. *J. Mater. Chem.* **2007**, *17*, 2329. (d) Jiang, Z.-Y.; Xie, Z.-X.; Zhang, X.-H.; Lin, S.-C.; Xu, T.; Xie, S.-Y.; Huang, R.-B.; Zheng, L. S. *Adv. Mater.* **2006**, *16*, 904.
(11) (a) Zhiu, H.; Fan, T.; Zhang, D.; Guo, Q.; Ogawa, H. *Chem. Mater.* **2007**, *19*, 2144. (b) Fujikawa, S.; Takaki, R.; Kunitake, T. *Langmuir* **2005**, *21*, 8899–8904. (c) Numata, M.; Sugiyasu, K.; Hasegawa, T.; Shinkai, S. *Angew. Chem., Int. Ed.* **2004**, *43*, 3279–3283. (d) Zhou, H.; Fan, T.; Zhang, D. *Microporous Mesoporous Mater.* **2007**, *100*, 322–327. (e) Begu, S.; Girod, S.; Lerner, D. A.; Jardiller, N.; Tourne-Peteilh, C.; Devoisselle, J.-M. *J. Mater. Chem.* **2004**, *14*, 1316.
(12) (a) Choi, W. S.; Koo, H. Y.; Zhongbin, Z.; Li, Y.; Kim, D.-Y. *Adv. Funt. Mater.* **2007**, *17*, 1743. (b) Caruso, F.; Schuler, C.; Kurth, D. G. *Chem. Mater.* **1999**, *11*, 3394. (c) Bourlinos, A. B.; Karakassides, M. A.; Petridis, D. *Chem. Commun.* **2001**, 1518.
(13) (a) Wong, M. S.; Cha, J. N.; Choi, K.-S.; Deming, T. J.; Stucky, G. D. *Nano Lett.* **2002**, *2*, 583. (b) Ma, Y.; Qi, L.; Ma, J.; Cheng, H. *Langmuir* **2003**, *19*, 4040. (c) Yh, Y.-Q.; Chen, B.-C.; Lin, H.-P.; Tang, C.-Y. *Langmuir* **2006**, *22*, 6. (d) Zhao, D.; Feng, J.; Huo, Q.; Melosh, N.; Fredrickson, G. H.; Chmelka, B. F.; Stucky, G. D. *Science* **1998**, *279*, 548. (e) Yang, P.; Zhao, D.; Margolese, D. I.; Chmelka, B. F.; Stucky, G. D. *Nature* **1998**, *396*, 152. (f) Chen, S.-Y.; Cheng, S. *Chem. Mater.* **2007**, *19*, 3041.
(14) (a) Xu, H.; Wei, W.; Zhang, C.; Ding, S.; Qu, X.; Liu, J.; Lu, Y.; Yang, Z. *Chem. Asian J.* **2007**, *2*, 828. (b) Yang, M.; Ma, J.; Zhang, C.; Yang, Z.; Lu, Y. *Angw. Chem. Int. Ed.* **2005**, *44*, 6727. (c) Yang, Z.; Niu, Z.; Lu, Y.; Hu, Z.; Han, C. C. *Angw. Chem. Int. Ed.* **2003**, *42*, 1943. (d) Caruso, F.; Caruso, R. A.; Mohwald, H. *Science* **1998**, *282*, 1111.
(15) (a) Sun, X.; Li, Y. *Angw. Chem. Int. Ed.* **2004**, *43*, 3827. (b) Sun, X.; Liu, J.; Li, Y. *Chem. Eur. J.* **2006**, *12*, 2039. (c) Titirici, M.-M.; Antonietti, M.; Thomas, A. *Chem. Mater.* **2006**, *18*, 3808. (d) Chang-Chien, C.-Y.; Hsu, C.-H.; Lee, T.-Y.; Liu, C.-W.; Wu, S.-H.; Lin, H.-P.; Tang, C.-Y.; Lin, C.-Y. *Eur. J. Inorg. Chen.* **2007**, 3798.
(16) Suarez, F. J.; Sevilla Alvarez, M. S.; Valdes-Solis, T.; Fuertes, A. B. *Chem. Mater.* **2007**, *19*, 3096.
(17) (a) Huang, C.-C.; Hwu, J. R.; Su, W.-C.; Shieh, D.-B.; Tzeng, Y.; Yeh, C.-S. *Chem. Eur. J.* **2006**, *12*, 3805. (b) Hsiao, M.-T.; Chen, S.-F.; Shieh, D.-B.; Yeh, C.-S. *J. Phys. Chem. B* **2006**, *110*, 205. (c) Sun, Y.; Xia, Y. *Science* **2002**, *298*, 2176. (d) Sun, Y. B.; Mayers, T.; Xia, Y. *Nano Lett.* **2002**, *2*, 481.
(18) Zhang, Y. Z.; Feng, Y.; Huang, Z.-M.; Ramakrishna, S.; Lim, C. T. *Nanotechnology* **2006**, *17*, 901.
(19) (a) Narayani, R.; Rao, K. P. *J. Appl. Polym. Sci.* **1995**, *58*, 1761. (b) El-Simaligy, M. S.; Rohdewald, P. *J. Pharm. Pharmacol.* **1983**, *35*, 537.

in 25 mL of water at 52 °C, added 0.2 mL of 4.5 M of HCl, and stirred the mixture for 3 min. Within the next 15 min, we added, dropwise, 48 mL of acetone to the solution. The mixture solution (1.5 g of gelatin, 25 mL of water, 0.2 mL of 4.5 M of HCl, and 48 mL of acetone) was then cooled to room temperature and 0.3 mL of water, 0.7 mL of acetone, and 0.2 mL of glutaraldehyde were added to the solution to initiate the cross-linking interaction. The gelatin-template formation reaction was stopped after 24 h. After centrifugation (6000 rpm for 10 min), the templates were washed three times with ethanol. The templates were then stored in ethanol for further use.

We also prepared a stock solvent by mixing isopropyl alcohol and toluene (ratio 1:2, v/v; hereafter called "IT solvents"), to fabricate hollow Gd_2O_3 nanospheres. Therefore, the solvent in the ethanol−gelatin was exchanged with equal volume of IT solvents for the hollow Gd_2O_3 nanospheres experiment and called "IT gelatin solution". To prepare P123 solution, we added 1.62 g of P123 to 82.5 mL of ethanol containing 5.4 mL of 4.5 M HCl, where the PEO groups were partially protonated in the acid solution.

Method 1. To make hollow Gd_2O_3 nanospheres, we added 0.075 mL of gadolinium isopropoxide solution to 10 mL of mixed and diluted IT gelatin solutions and 0.075 mL of P123 solution, stirred it continuously for 3 h, and then heated the resultant solution to 88 °C for 14−16 h with a temperature-controlled oven. While the mixture solution (0.075 mL of gadolinium isopropoxide, 10 mL of diluted IT gelatin solutions, and 0.075 mL of P123 solution) was being hydrothermally heated, the hand-shaking step occurred every 45 min for the initial 6−8 h, but not for the final 7−8 h. The hollow Gd_2O_3 nanospheres were then washed with a solvent five times using centrifugation at 6000 rpm for 10 min. The washed samples were dried in air and calcinated at 580 °C for 2 h in air. The above-diluted IT gelatin solutions were prepared by adding 1 mL of IT gelatin solution to 9 mL of pure IT solution. Gelatin templates can be removed using either simple calcination or hot water treatments. We prefer calcination to form in situ crystalline oxide. TGA analysis indicated that pure gelatin core can be removed at 683 °C. In fact, the organic core of the gelatin/inorganic composite was removed at 580 °C, which is lower than the removal temperature of the pure gelatin core (683 °C), during calcination when forming hollow Gd_2O_3 (Supporting Information, Figure S1).

To fabricate hollow TiO_2 nanospheres, we used ethanol as a solvent. We first prepared 10 mL of diluted ethanol−gelatin solution by combining 0.5 mL of ethanol−gelatin and 9.5 mL of ethanol. Next, we slowly added 37.5 μL of titanium isopropoxide to the 10 mL of diluted ethanol−gelatin solution, which was then stirred for 12 h. The TiO_2 nanospheres were washed using centrifugation with ethanol, dried, and then calcinated in air at 580 °C for 2 h.

Method 2. We prepared porous Gd_2O_3 nanospheres by mixing 0.1 mL of $GdCl_3$ (0.2 M), 3.5 mL of P123 solution, and 8 mL of diluted ethanol−gelatin solutions together for 1 h and then pouring the mixture into a glass dish (11 cm in diameter). We next transferred the loaded disk to an oven set at 36 °C for 16−24 h to ensure that the solvent completely evaporated. We prepared the diluted ethanol−gelatin solutions by adding 0.8 mL of ethanol−gelatin to 7.2 mL of ethanol. After the mixture had dried, it was calcinated at 580 °C for 2 h to produce porous Gd_2O_3 nanospheres.

To prepare porous TiO_2 nanospheres, we added 0.075 mL of titanium isopropoxide to 11.5 mL of gelatin/P123 solutions (3.5 mL of P123 solution and 8 mL of diluted ethanol−gelatin solutions) and stirred it continuously for 1 h. To ensure that the solvent completely evaporated, we poured the mixture into a glass dish (11 cm in diameter) and transferred the loaded disk to an oven set at 36 °C for 16−24 h. After the mixture had dried, it was calcinated at 580 °C for 2 h.

Biocompatibility of Hollow and Porous Gd_2O_3 Nanospheres in in Vitro Tests. *Leaching Gd^{3+} Ions Test.* Hollow and porous Gd_2O_3 nanospheres were introduced into distilled water by sonicating in an ultrasonic bath for 30 min to prepare Gd_2O_3 suspensions (1.1 mM). Then, the suspensions were stored at 4 °C. After storage at 4 °C for 8 days, the suspensions were centrifuged using 13 000 rpm for 30 min at 4 °C to eliminate precipitates. Subsequently, the supernatants were analyzed using an inductively coupled plasma atomic emission spectrometer (ICP-AES, Jobin Yvon JY138 Spectroanalyzer). The same procedures were conducted for Gd_2O_3 suspensions stored at 37 °C for 8 days.

The Biocompatibility of Hollow and Porous Gd_2O_3 Nanospheres. We treated a Vero (monkey kidney) cell line with Gd_2O_3 nanospheres and then used WST-1 (tetrazolium salt) and MTT (3-(4,5-dimethylthiazol-2-yl)-2,5-diphenyltetrazolium bromide) assays to determine the biocompatibility of the nanospheres. Briefly, the Vero cells were cultured in a 96-well microplate with modified Eagle's medium (MEM) containing 10% fetal bovine serum (FBS), 1% L-glutamine, 1% pyruvate, 1% nonessential amino acid, and 1% penicillin/streptomycin/neomycin (PSN). The initial density was 4×10^3 cells/well. The cells were maintained at 37 °C in a humid atmosphere of 95% air and 5% CO_2. After 24 h, serial diluents of the hollow and porous Gd_2O_3 nanospheres at concentrations of 200, 100, or 10 $\mu g/mL^{-1}$ were added to the culture wells to replace the original culture medium with a final volume of 100 μL. The cells were incubated with the particles for 24 h. The culture medium was then removed and replaced by 100 μL of fresh culture medium containing 10% WST-1 reagent for the WST-1 assay and MTT reagent for the MTT assay. The cells were then incubated at 37 °C for 1.5 h for the WST-1 assay and 4 h for the MTT assay to allow formazan dye to form. Next, the cultural medium in each well was centrifuged (to prevent the nanoparticles from interfering with the spectrophotometric measurement) and then transferred to an ELISA plate. The quantification determining cell viability was done using an ELISA plate reader at an optical absorbance of 450/690 nm for the WST-1 assay and 540/650 nm for the MTT assay.[5,6]

Preparing Hollow and Porous Gd_2O_3 Nanosphere Samples for MR Assays. *In Vitro MR Imaging.* The experiments were done using a spectroscope (3 T MRI Biospec, Bruker, Ettlingen, Germany). We prepared the samples in the same way as previously described.[5] A gradient system mounted on the table of the 3 T magnet with an inner diameter of 6 cm and a maximal gradient strength of 1000 mT m^{-1} was used to yield high-resolution images. A quadrature coil with an inner diameter of 3.5 cm was used for RF transmission and reception. For T_1 and T_2 measurements, both hollow and porous Gd_2O_3 nanospheres with various Gd^{3+} concentrations (0, 0.01, 0.03, 0.06, 0.08, 0.11, 0.14, 0.28, 0.55, 0.83, 1.10, and 1.38 mM) were dispersed in 0.5% agarose gel. The acquired MR images had a matrix size of 256 × 192, a field of view of 70 × 70 mm^2, and a slice thickness of 6 mm, yielding an in-plane resolution of 273 μm after image smoothing. Both T_1- and T_2-weighted images were acquired using a multislice multiecho (T_1-weighted) and fast spin−echo (T_2-weighted) sequence with a repetition time/echo time (TR/TE) of 427.1/9.3 ms and a number of averages (NEX) of 10 (T_1) and TR/TE of 4500/62.7 ms and a NEX of 5 (T_2). T_1 value measurements were done using a multislice multiecho sequence with a TR of 6000 ms, a TE of 8.7 ms, and 45 inversion−recovery points (TI from 13.3 to 6000 ms). The field of view was 70 × 70 mm^2, the slice thickness was 6 mm, and the image matrix was 128 × 128. This allowed for simultaneous imaging of 24 vials with 0.3 mL of contrast agent for each vial. An average signal of 50 voxels was evaluated for all TI values. T_2 value measurements were performed with a spin−echo sequence of TR/TE of 4000/10.1 ms, 60 echo points of different 60 echo

time, and a NEX of 5. The field of view was 60 × 60 mm^2, the slice thickness was 6 mm, and the imaging plane was 256 × 192.

Characterization. The crystalline structures were identified using an X-ray diffractometer (XRD-7000S; Shimadzu Corp., Tokyo, Japan) with Cu Kα radiation (λ = 1.540 60 Å) at 30 kV and 30 mA. Electron micrographs of the samples were taken using transmission electron microscopes (TEM) (JEOL 2010, at 200 kV, and PHILIPS CM-200, at 200 kV): we placed a drop of the sample on a copper mesh coated with an amorphous carbon film and then evaporated the solvent in a vacuum desiccator. Field emission scanning electron microscopic (FE-SEM) images of the hollow and porous nanospheres on a Cu plate substrate were taken using an FE-SEM at 10 kV (XL-40FEG; Philips). IR spectra were measured using a Fourier transformation infrared spectrometer (200E, JASCO International Co., Ltd., Tokyo, Japan) with a KBr plate. The Raman spectra were obtained using a Renishaw inVia Raman microscope equipped with a 632.8-nm air-cooled He−Ne laser (17 mW) as the excitation source. The samples were deposited on a clean glass substrate. A UV−vis spectrophotometer (Hewlett-Packard 8452A) was used for the Gd^{3+} ion leaching test. N_2 adsorption measurements were done at 77 K using an accelerated surface area and a porosimetry analyzer (ASAP 2010; Micromeritics Instrument Corp., Norcross, GA). We used Brunauer−Emmett−Teller (BET) calculations for the surface area and Barret−Joyner−Halenda (BJH) calculations for the pore-size distribution of dry-form powders from the adsorption branch of the isotherm. The hollow and porous Gd_2O_3 nanospheres were magnetized ($M-H$ loops) at 300 K with applied fields of up to 20 kOe using a Quantum Design MPMS-7 SQUID magnetometer. The ZFC and FC magnetization curves in a temperature range between 5 and 300 K at a 500 Oe applied field and the magnetization as a function of the applied field at temperature from 5 to 300 K in field between −20 and 20 kOe have been measured for hollow Gd_2O_3 nanospheres. The ζ-potential of the gelatin template dispersing in an aqueous solution was measured using a Zetasizer analyzer (Malvern, UK). This sample was prepared by exchanging the original solvent with deionized water (pH = 6.4, 18.2 mΩ), centrifuging the template, and then redispersing it. The pH value of the solution was determined to be 3.9 prior to ζ-potential measurement. Finally, we did a thermogravimetric analysis (TGA) using approximately 10 mg of sample on a NETZSCH TG209 thermogravimetric analyzer at a heating rate of 10 °C/min under dried air.

Results and Discussion

In the present study, we used two different approaches to prepare superparamagnetic hollow and paramagnetic porous Gd_2O_3 nanospheres (Scheme 1). In method 1 a sol−gel process was to hydrolyze organometallic gadolinium isopropoxide over the gelatin cores under hydrothermal conditions. However, the porous Gd_2O_3 nanospheres were synthesized using method 2, where precursor deposition was induced by solvent evaporation, with gadolinium chloride as the precursor. The detailed synthesis processes are described in the Experiment Section. P123 was used in both methods to assist the formation of hollow and porous Gd_2O_3 nanospheres. The organic gelatin templates were removed using calcination in both methods 1 and 2, which resulted in hollow and porous spheres.

The gelatin template was synthesized by adding glutaraldehyde (GA),[20] a chemical cross-linker that can interact with amide, amine, or the carbonyl groups of gelatin.[21] The size of the gelatin template varied with the reaction time: 6 h (∼190.7 nm), 13 h (∼269.9 nm), and 24 h (∼385.3 nm). We created spherical gelatin templates using a 24-h reaction time (SEM image, Supporting Information, Figure S2a). IR analysis confirmed vibration peaks of amide I, amide II, and amide III for the gelatin templates (Supporting Information, Figure S3). The negative surface charge (−20.34 mV) of the gelatin templates was determined using ζ-potential. After the sol−gel process (method 1), a SEM image of the gelatin/inorganic composite revealed its well-defined shape (Supporting Information, Figure S2b).

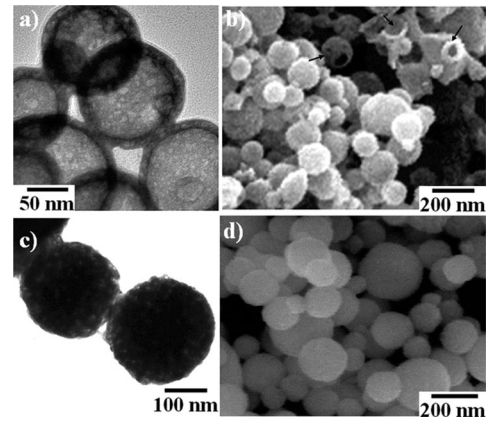

Figure 1. TEM and SEM of (a and b) hollow Gd_2O_3 nanospheres and (c and d) porous Gd_2O_3 nanospheres.

Figure 1 [TEM (a and c) and SEM (b and d) images] shows the morphologies and spherical shape of the hollow and porous Gd_2O_3 nanospheres. The interior of the hollow Gd_2O_3 nanospheres is lighter than the periphery (Figure 1a), which suggests a core-free nanostructure. SEM image shows that some particles are broken (marked by black arrows in Figure 1b) and supported the interior cavity morphology. The hollow Gd_2O_3 nanospheres were calculated to have a particle size of ∼133 nm and a shell thickness of ∼20.9 nm after counting 150 particles. Consequently, the diameter of the interior cavity is suggested to be ca. 91 nm. This shrinkage, a decrease in diameter to 35% of the original template, may relate to the intrinsic nature of the loosely cross-linked structure in the gelatin core and the low mechanical strength of the inorganic coating layer, as was shown for those using glucose condensed to form carbon materials as a template.[15a,b] The porous Gd_2O_3 nanospheres (∼186.7 nm in diameter calculated based on 150 particles) synthesized using method 2 (Figure 1c) appear solid. The particles possessed many nonordered pores of 3−12 nm that seemed to correspond with mesoporous nanostructures. The surface of the porous Gd_2O_3 nanospheres is smooth (Figure 1d). Both the hollow and porous spheres were characterized as polycrystal structures from the selected area ED pattern (Supporting Information, Figure S4).

X-ray diffraction (XRD) patterns allowed us to determine the crystal phase and crystalline structure of the as-obtained Gd_2O_3 nanomaterials (Figure 2a). Porous Gd_2O_3 nanospheres had higher intensity and narrower diffraction peaks than

(20) Coester, C.; Bon Briesen, H.; Langer, H.; Kreuter, J. *J. Microencapsulation* **2000**, *17*, 187.
(21) Jastrzebska, M.; Wrzalik, R.; Kocot, A.; Zalewska-Rejdak, J.; Cwalina, B. *J. Biomater. Sci. Polym. Ed.* **2003**, *14*, 185.

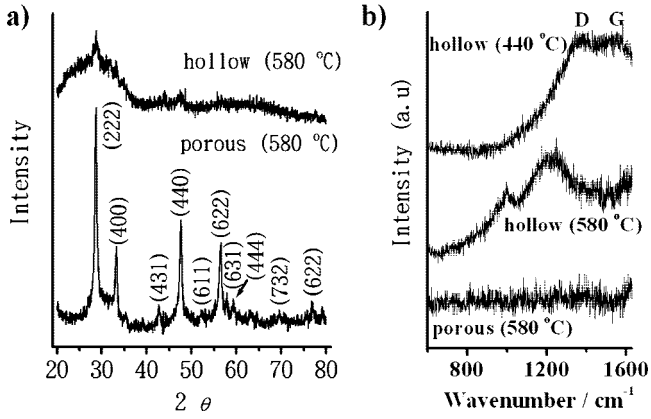

Figure 2. (a) XRD patterns of hollow and porous Gd_2O_3 nanospheres and (b) Raman spectra of hollow Gd_2O_3 nanospheres calcinated at 440 and 580 °C and the porous Gd_2O_3 nanospheres calcinated at 580 °C.

hollow Gd_2O_3 nanospheres. All peaks in the XRD patterns based on JPCDS No. 00−011−0604 resulted from the cubic Gd_2O_3 phase, and no impurity peaks were found. The unit cell constants were calculated with the values of $a = 10.78$ and 10.79 Å for hollow and porous Gd_2O_3 nanospheres, respectively, which are consistent with the literature value (10.82 Å). Grain sizes of 12.0 nm for hollow and 27.5 nm for porous Gd_2O_3 nanospheres were estimated from the main peak of (222).

A broadened band at the (222) peak of hollow Gd_2O_3 nanospheres at 20−37° (Figure 2a) was attributed to carbon materials.[22] The carbon coating is generated possibly because of incomplete prolysis of the gadolinium isopropoxide precursor during calcination. At the lower calcination temperature of 440 °C, method 1 resulted in black products, and the color was consistent with a previous report using gadolinium isopropoxide as a precursor to prepare a thin film.[23] The carbon products generated at 440 °C in our experiment were measured using a Raman spectrum (Figure 2b). The labels of the D- and G- bands at ∼1340 and ∼1570 cm^{-1} were ascribed to the carbon material. It had been reported that the G band was related to sp^2-hybridized carbon atoms, as in a graphite layer, and that the D band originated from disordered graphite.[24] The forms of both bands were identical to carbon. When the temperature was raised to 580 °C, the G line disappeared and the D line red-shifted, which resulted in broadened peaks at 1230 and 1000 cm^{-1}. Although we were unable to identify those peaks at this stage, their broad shape indicated that they might have been the result of residual carbon species from incomplete decomposition of carbon products. Nevertheless, we did not find the broadened Raman signal for porous Gd_2O_3 nanospheres prepared at 580 °C (Figure 2b).

The thermogravimetric analysis has been carried out for hollow and porous Gd_2O_3 particles (Supporting Information, Figure S5). A two-step weight loss of 4% was observed between 45 and 450 °C and a sequent loss of 0.8% in the range of 450−475 °C for hollow Gd_2O_3. On the other hand,

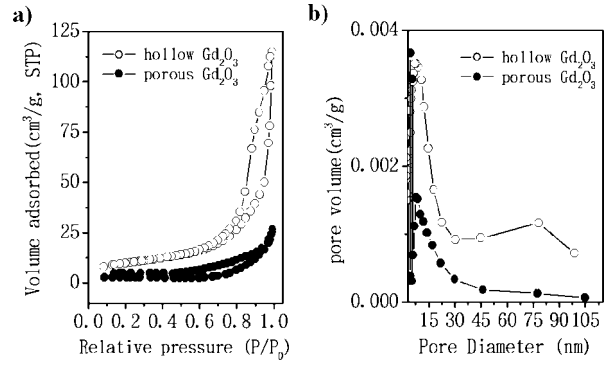

Figure 3. Nitrogen adsorption−desorption isotherms (a) and corresponding pore-size distributions (b) for hollow and porous Gd_2O_3 nanospheres.

a one-step weight loss of 2.3% (45−450 °C) was determined in porous Gd_2O_3 spheres. The weight-loss profile that occurred between 45 and 450 °C could be attributed to elimination of physical adsorbed water (below 200 °C) and chemisorbed water (above 200 °C).[25] The residual carbon coating on hollow Gd_2O_3 particles could be completely burnt away when the temperature increased up to 750 °C. Therefore, the weight loss determined the residual carbon as 0.8%. The weight fraction of the residual carbon in the hollow Gd_2O_3 spheres was calculated as 0.83% after removal of physical and chemisorbed water.

We used the gas adsorption−desorption method to confirm the porosity of porous and hollow as-synthesized Gd_2O_3 nanospheres. Figure 3a shows the N_2 adsorption−desorption isothermal plots of the hollow and porous Gd_2O_3 nanospheres. The surface area of the hollow Gd_2O_3 nanospheres calculated using the BET plot was 35.2 $m^2\ g^{-1}$, which is higher than the value of porous Gd_2O_3 nanospheres (8.7 $cm^2\ g^{-1}$). For the N_2 adsorption−desorption of hollow Gd_2O_3 nanospheres, the type IV isotherm, with an H2 hysteresis at relatively higher pressure (P/P_0 of 0.8−1), indicates the macroporous character while the type IV isotherm branching at relatively lower pressure (P/P_0 of 0.5−0.95) in the porous Gd_2O_3 nanospheres indicates the mesoporous character. Figure 3b gives the pore size distributions for both hollow and porous Gd_2O_3 nanospheres. Using the BJH method, we found, at relatively higher pressure (P/P_0), a distinct hysteresis loop of the hollow Gd_2O_3 nanospheres that corresponded to the large pores (range of 50−105 nm) in the hollow macroporous interior. These macropores were centered at 78.3 nm, which is close to the diameter of the interior cavity from TEM measurement and accompanied the small pores centered at 7.8 nm. For the porous Gd_2O_3 nanospheres, however, we found two distinct pore distribution peaks at 4.4 and 7.8 nm that indicated their mesoporous character.

When we applied an external magnetic field, both hollow and porous nanospheres could be dragged (Supporting Information, Figure S6). Figure 4a shows SQUID magnetometry magnetization−magnetic field ($M-H$) plots at 300 K. We found that hollow and porous Gd_2O_3 nanospheres had different magnetic properties. As the strength of the

(22) Li, Z.; Jaroniec, M.; Papakonstantnou, P.; Tobin, J. M.; Vohrer, U.; Kumar, S.; Attard, G.; Holmes, J. D. *Chem. Mater.* **2007**, *19*, 3349.
(23) Garcia-Murillo, A.; Le Luyr, C.; Dujardin, C.; Pedrini, C.; Mugnier, J. *Opt. Mater.* **2001**, *16*, 39.
(24) Ferrari, A. C.; Robertson, J. *Phys. Rev. B* **2000**, *61*, 14095.
(25) (a) Guo, Z.; Pereira, T.; Choi, O.; Wang, Y.; Hahn, H. T. *J. Mater. Chem.* **2006**, *16*, 2800. (b) Oliverira, M. M.; Schnitzler, D. C.; Zarbin, A. J. G. *Chem. Mater.* **2003**, *15*, 1930.

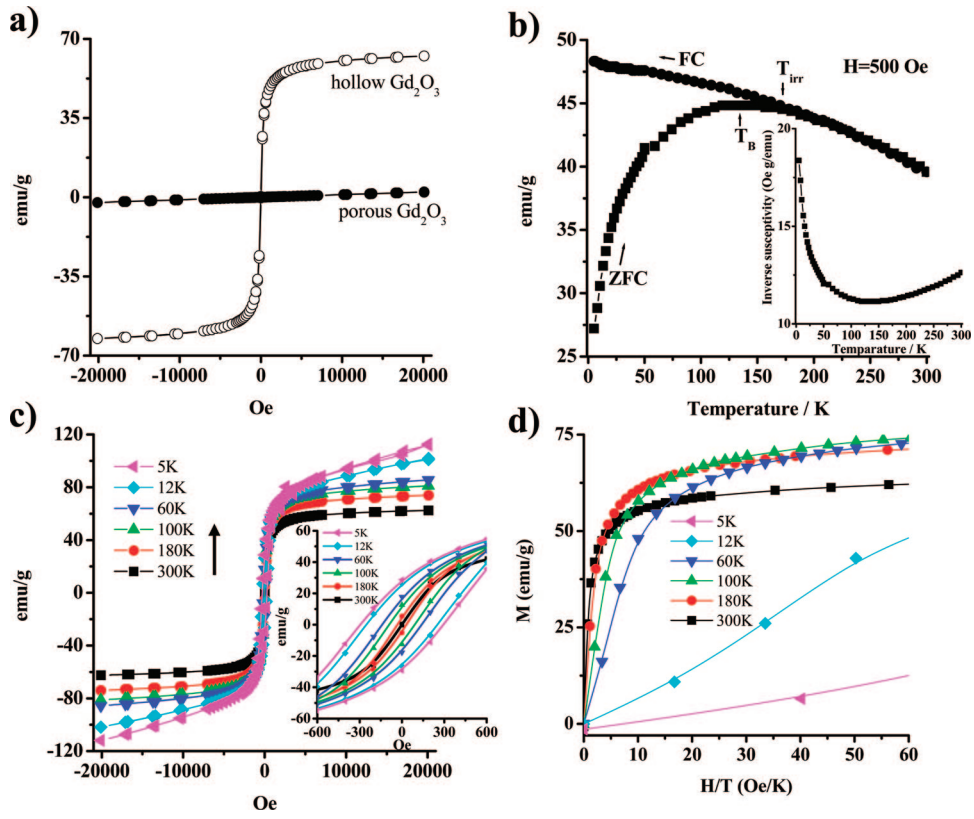

Figure 4. (a) Magnetization plots of hollow and porous Gd_2O_3 nanospheres as a function of the applied fields (−20 and + 20 kOe) at 300 K. (b) Temperature-dependent ZFC-FC magnetization curves measured at 500 Oe for hollow Gd_2O_3 nanospheres. The inset shows the inverse susceptibility χ^{-1}(ZFC) vs T plot. (c) Magnetization vs H dependence of hollow Gd_2O_3 nanospheres in the fields (−20 and + 20 kOe) at different temperatures from 5 to 300 K. The inset shows the enlarged view in the fields between −600 and 600 Oe. (d) Magnetization vs H/T shown at 5, 12, 60, 100, 180, and 300 K.

applied magnetic field increased, the linear correlation between the magnetization and the applied magnetic field in the porous Gd_2O_3 nanospheres indicated paramagnetism. In contrast, the hollow Gd_2O_3 nanospheres show a steep slope and the lack of a hysteresis loop in the $M-H$ plot, indicating superparamagnetism. It should be mentioned that a very little amount of ~1.2 μg of Gd^{3+} ions leaching out of hollow or porous Gd_2O_3 powders (4 mg), as determined by ICP analysis after SQUID performance. On the basis of the TGA measurements, the magnetic moments (emu/g) were determined after subtraction of physical and chemisorbed water and residual carbon on hollow Gd_2O_3 surface. This has resulted in a magnetic moment of 62.4 emu/g at 20 kOe for hollow Gd_2O_3 particles. To gain insight into the superparamagnetic property for hollow Gd_2O_3 particles, the temperature dependence of magnetization ZFC-FC curves were measured. Figure 4b shows the temperature dependence of ZFC-FC magnetization plots measured in a temperature range between 5 and 300 K at a 500 Oe applied field. ZFC magnetization increases as the temperature rises from 5 K and reaches a maximum at the blocking temperature T_B = 135 K. The ZFC and FC curves are irreversible below the irreversible temperature T_{irr} = 170 K, which is defined as the blocking temperature of particles with the highest energy barrier. Figure 4b presents typical behavior of superparamagnetic particles. The inset of Figure 4b displays the variation in inverse magnetization with temperature for hollow Gd_2O_3 particles. This figure shows that, above T_B, the data does not fall on a straight line and χ_{ZFC} does not follow the Curie−Weiss law, $\chi_{ZFC}\alpha(T-\theta)^{-1}$, giving rise to large negative θ = −697 K. It has been suggested that such non-Curie−Weiss behavior for $T > T_B$ could be attributed to strong dipolar interaction between particles.[26,27] Figure 4c shows the variation of magnetization loops for hollow Gd_2O_3 at temperatures from 5 to 300 K in a field between −20 and 20 kOe. The magnetic moment decreases from 111.9 to 62.4 emu/g at 20 kOe as temperature increases from 5 to 300 K. Furthermore, the remanence magnetization (M_r) and coercivity (H_c) decrease from 28.7 emu/g and 300 Oe, respectively, to zero as the temperature increases from 5 to 300 K. The inset of Figure 4c displays the zoom region between −600 and 600 Oe to show more clearly the hysteresis loop. For temperature $T \leq$ 100 K (5, 12, 60, and 100 K), the $M(H)$ hysteresis loops are irreversible, while the irreversibility of the hysteresis loop is extremely small, suggesting almost superparamagnetic behavior, at 180 K. The hysteresis loop areas gradually decrease as temperature increases from 5 to 180 K, indicating a transition of ferromagnetic to superparamagnetic state. The zero coercivity and zero remanent magnetization feature at 300 K indicate the presence of superparamagnetic behavior. The plots of M versus H/T for T = 5, 12, 60, 100, 180, and 300 K are

(26) Leslie-Pelecky, D. L.; Pieke, R. D. *Chem. Mater.* **1996**, *8*, 1770.
(27) (a) Wang, H.; Zhang, F.; Zhang, W.; Wang, X.; Lu, Z.; Qian, Z.; Sui, Y.; Donag, D.; Su, W. *J. Cryst. Growth* **2006**, *293*, 169. (b) Hou, Y.; Yu, J.; Gao, S. *J. Mater. Chem.* **2003**, *13*, 1983. (c) Garcia-Otero, J.; Poto, M.; Rivas, J.; Bunde, A. *Phys. Rev. Lett.* **2000**, *84*, 167. (d) Chantrell, R. W.; Walmsley, N. *Phys. Rev. B* **2000**, *63*, 024410–1. (e) Mamiya, H.; Nakatani, I.; Furubayashi, T. *Phys. Rev. Lett.* **1998**, *80*, 177. (f) Seehra, M. S.; Babu, V. S.; Manivannan, A. *Phys. Rev. B* **2000**, *61*, 3513.

shown in Figure 4d. Plotting the magnetization against H/T shows that the curve profiles gradually changed from 5 to 300 K.

Superparamagnetic particles magnetize strongly under an applied magnetic field, but they retain no permanent magnetism once the field is removed. As in previous investigations of superparamagnetic iron oxides,[3,4,28] superparamagnetic Gd_2O_3 may potentially be used in applications with ferrofluids, for biomedical detection (MRI), separation (cells, DNA, and proteins), drug delivery, and magnetically induced hyperthermia. Why does hollow Gd_2O_3 exhibit superparamagnetic behavior? Notably, the materials with partially filled d or f electron orbits that surface capping material with organic compounds influence their intrinsic magnetic properties.[29] One study[29a] reported the transformation from a diamagnetic gold (Au) metal core to a ferromagnetic Au composite because of the surface Au−sulfur (S) bond after the surface had been coated. This phenomenon was attributed to the size effect and to the spin of extra d holes generated near the Au−S bond, which gives rise to localized magnetic moments. Another study[29b] recently reported that modifying the surface of O, N, and S atoms in zinc oxide (ZnO) nanoparticles (~10 nm) strongly influenced the magnetism because of the alteration of the electronic configuration originating from ZnO. In our Raman monitor (Figure 2b), carbon residuals were generated. We hypothesized that the organic layer caused the superparamagnetism. Some studies have reported that the magnetic behaviors of lanthanide oxide nanoparticles could be affected by surface coating.[30,9c] For example, superparamagnetic-like characteristic was found in dextran-coated Gd_2O_3 nanoparticles.[9c] In fact, we have found that the superparamagnetic hollow Gd_2O_3 converted to paramagnetic state after removal of the residual carbon on the surface by calcination of hollow Gd_2O_3 at 800 °C (Supporting Information, Figure S7). Hysteresis plot ($M-H$) analysis result shows that the calcined hollow Gd_2O_3 particles (800 °C) exhibited a nearly linear correlation between the magnetization and the applied magnetic field at 300 K. The ZFC-FC curve ($M-T$ plot) under 1 kOe for calcined hollow Gd_2O_3 is similar to previously reported $M-T$ graphs obtained with paramagnetic Gd_2O_3 nanoparticles.[9a,c]

Because of their hollow and porous structures, these Gd_2O_3 nanomaterials favor proton coordination and water exchange. We then evaluated whether hollow or porous Gd_2O_3 nanospheres were usable as contrast agents in magnetic resonance imaging (MRI). We did in vitro MR assays (T_1- and T_2-weighted imaging) in 0.5% agarose gel for both types of nanospheres using a series of Gd concentrations (range 0−1.38 mM). The proton relaxivities r_1 and r_2 of hollow and porous nanospheres were determined from the longitudinal (T_1^{-1}) and transverse (T_2^{-1}) relaxation rates at various

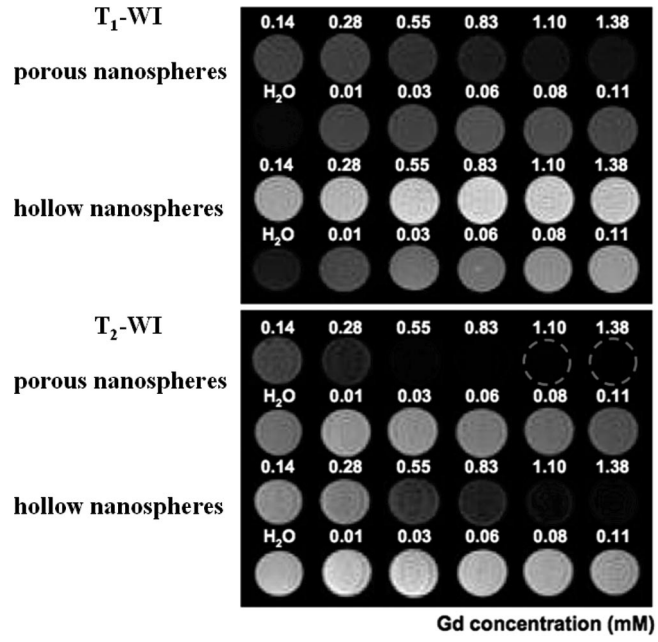

Figure 5. T_1- and T_2-weighted images of hollow and porous Gd_2O_3 nanospheres with various Gd^{3+} concentrations.

concentrations using a 3 T MRI system. When the concentrations were increased, T_1-weighted images became brighter, and the signal intensity of hollow nanospheres increased ~268% from 0 to 1.10 mM (Figure 5). On the other hand, the signal intensity of porous nanospheres increased only ~142% from 0 to 0.14 mM, and the intensity gradually decreased as the particle concentration increased to 1.38 mM (Supporting Information, Figure S8a). The relaxivity (r_1) values of hollow and porous nanospheres were 17.7 and 16.8 s^{-1} mM^{-1}, respectively (Supporting Information, Figure S9 and S10). In T_2-weighted imaging, both hollow and porous Gd_2O_3 nanospheres made the images darker at higher Gd concentrations (Figure 5), and the signal intensities decreased ~78% for hollow nanospheres and ~96% for porous nanospheres (Supporting Information, Figure S8b). The r_2 values were 26.6 s^{-1} mM^{-1} for hollow nanospheres and 31.4 s^{-1} mM^{-1} for porous nanospheres. The ratio of r_2/r_1 is the reference value for MR positive contrast agent enhancement. The closer the r_2/r_1 value is to 1, the higher the positive contrast enhancement. In the present study, the r_2/r_1 value was 1.50 for hollow nanospheres and 1.87 for porous nanospheres; therefore, the hollow nanospheres produced better T_1 contrast enhancement. In the gas adsorption−desorption assay, the surface areas of the hollow nanospheres were larger than those of the porous nanospheres. Because of this, more water reached the inner surface of hollow nanospheres, increased the interaction between water and Gd^{3+} ions, and brightened the T_1-weighted images. We have also evaluated a commercially available Gd−DTPA and found that, at the 3 T field, it had an r_1 value of 9.2 s^{-1} mM^{-1}, almost half the r_1 values of our nanospheres. Because of the possible contribution to proton relaxivity from leached out Gd^{3+} ions, the nanoparticle suspensions were measured by ICP analysis after in vitro MRI measurements. A very small amount of free Gd^{3+} of 17.2 and 32.4 μM were determined from hollow and porous nanoparticles (both with 1 mg/mL of Gd_2O_3 corresponding to 5.5 mM of Gd^{3+} ions), respectively. The

(28) Jeong, U.; Teng, X.; Wang, Y.; Yang, H.; Xia, Y. *Adv. Mater.* **2007**, *19*, 33.
(29) (a) Crespo, P.; Litran, R.; Rojas, T. C.; Multigner, M.; De la Fuent, J. M.; Sanchez-Lopez, J. C.; Garcia, M. A.; Hernando, A.; Penades, S.; Fernandez, A. *Phys. Rev. Lett.* **2004**, *93*, 087204–1. (b) Garcia, M. A.; Merino, J. M.; Fernandez Pinl, E.; Quesada, A.; De la Venta, J.; Ruiz Gonzalz, M. L.; Castro, G. R.; Crespo, P.; Llopis, J.; Gonzalez-Calbt, J. M.; Hernando, A. *Nano Lett.* **2007**, *7*, 1489.
(30) Norek, M.; Pereira, G. A.; Geraldes, C. F. G. C.; Denkova, A.; Zhou, W.; Peters, J. A. *J. Phys. Chem. C* **2007**, *111*, 10240.

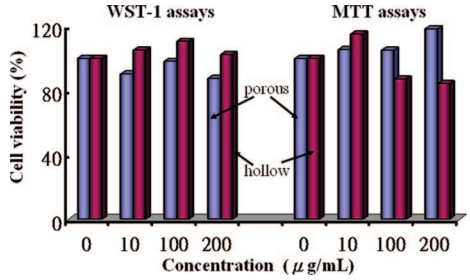

Figure 6. Biocompatibility of the hollow and porous Gd_2O_3 nanospheres estimated using WST-1 and MTT assays.

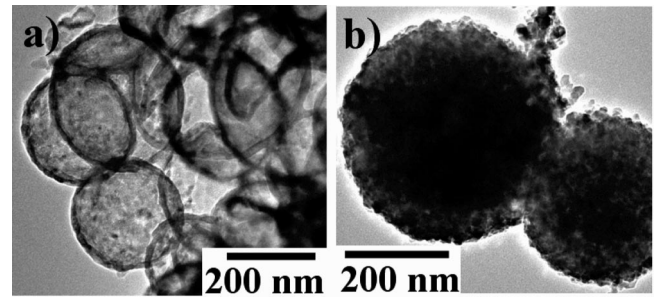

Figure 7. TEM images of (a) hollow and (b) porous TiO_2 nanospheres.

proton relaxivity values contributed from leached out Gd^{3+} ions would be very little.

Gd-based materials including Gd^{3+} ions are cytotoxic. Therefore, it was necessary to investigate the stability of the hollow and porous Gd_2O_3 nanopsheres and monitor cell viability. The leaching experiments were conducted to study the stability of as-prepared Gd_2O_3 particles after they had been incubated at 4 and 37 °C for 8 days (Supporting Information, Figure S11). By ICP analysis, we found that a very small amount of free Gd^{3+} of 20 and 27 μM leached out from hollow and porous nanospheres (both with 1.1 mM of Gd_2O_3 corresponding to 2.2. mM of Gd^{3+} ions), respectively, at 4 °C while the free Gd^{3+} ions were determined as 33 μM for hollow Gd_2O_3 and 43 μM for porous ones at 37 °C. In addition, the biocompatibility, cell viability experiments were conducted on a Vero (monkey kidney) cell line, using two well-established WST-1 and MTT assays (Figure 6). The nanospheres were tested at a range (0−200 μg/mL) of doses. Both assays yielded satisfactory biocompatibility at all doses for both hollow and porous nanospheres. This was consistent with the findings in our leaching study and might imply that the nanospheres are relatively noncytotoxic in vivo. More cytotoxicity studies are required to confirm this, however.

Gd_2O_3 nanospheres were used to illustrate the basic approaches in this work (Scheme 1). Initially, the gelatin particles were formed by adding a GA cross-linker. Polypeptide $-COO^-$ groups dominated the surface properties of the gelatin particles. The IR spectrum supported the presence of carboxylic groups in the gelatin core (Supporting Information, Figure S3). This functional group was thus considered a metal ion chelating agent through electrostatic attraction. When forming hollow Gd_2O_3 nanospheres using method 1, condensed gadolinium isopropoxide coated the thin layers on the carboxyl group sites of the gelatin. We used a solvent composed of isopropyl alcohol and toluene (2:1) in this synthesis because it stabilizes the inorganic precursor of gadolinium isopropoxide. In the course of the reaction, hydrolysis and condensation reactions combined with hydrothermal treatment (hydrothermally heated in a sealed vessel at 88 °C for 14−16 h) induced the thin layer to gradually transform into a solid shell. In the final stage, we used calcination at 580 °C to remove the organic cores, as the layers of coating were transformed into crystalline Gd_2O_3. Without hydrothermal treatment, hollow Gd_2O_3 nanospheres barely formed (Supporting Information, Figure S12). To form porous Gd_2O_3 nanospheres using method 2, a slow solvent evaporation induced gadolinium chloride deposition. The gelatin template used in our system consisted of polypeptides loosely packed in the form of cross-linking structures. The templates thus allowed the solvents and solutes to penetrate the biological cores during the diffusion- and capillarity-driven solvent evaporation. Finally, the gelatin template adsorbed with Gd^{3+} ions was calcinated and left a crystallized but porous Gd_2O_3 frame. The P123 polymer comprised of a hydrophilic ethylene oxide (EO) group and a hydrophobic propylene oxide (PO) group is critical for forming Gd_2O_3 nanospheres in both methods 1 and 2. In the control experiments, Gd_2O_3 nanomaterials were prepared using methods 1 and 2 without P123. This resulted in the formation of a great many small particle aggregations but no hollow or porous Gd_2O_3 nanospheres (Supporting Information, Figure S13). In the acid solution, it is believed that the EO group of P123 is protonated[31] and adsorbed onto the negatively charged gelatin template. Thus, P123 polymers not only result in good dispersion of the templates in the organic solvent but also help precipitate inorganic gadolinium precursors on the gelatin during the sol−gel process or solvent evaporation by means of surface coordination.[13e] Although IR analysis was used to monitor P123 polymer in the gelatin/inorganic composite, the vibration peaks of the P123 polymer were not apparent (Supporting Information, Figure S3). This may have occurred because the P123 layer in the gelatin/inorganic composite was too thin to be detected or because of peak overlap, or both, with the gelatin templates.

Gelatin templates are promising for preparing hollow and porous nanospheres. They have several advantages: they (1) are inexpensive, (2) are simple to prepare and easy to scale up to the gram level, (3) are adjustable in size, (4) have a multifunctional carboxylic group for electrostatic, amphiphilic, and chelating interactions to metal sources, and (5) allow easy surface modification using chemical binding or electrostatic attractions. We have also used these methods 1 and 2 (Scheme 1) to prepare hollow and porous TiO_2, such as hollow TiO_2 (particle sizes of ∼260.2 nm) and porous TiO_2 (particle sizes of ∼313.6 nm) (TEM images, Figure 7). We describe how we prepared those samples in the Experimental Section. The hollow TiO_2 nanospheres (Figure 7a) were obtained following the simple sol−gel process (method 1). The average shell thicknesses of the hollow nanospheres were estimated to be ∼14.68 nm for TiO_2. The morphology of porous TiO_2 nanospheres (Figure 7b) prepared with method 2 was like that of the porous Gd_2O_3

(31) Chen, S. Y.; Cheng, S. *Chem. Mater.* **2007**, *19*, 3041.

nanospheres (Figure 1c): they had many nonordered pores. We took N_2 adsorption−desorption measurements for porous TiO_2 and determined that the BET surface area was 41.6 m^2 g^{-1}. Using the BJH method, we found that the pore size distribution was centered at 6.8 nm (mesoporous) for porous TiO_2 nanospheres (Supporting Information, Figure S14). XRD analysis of the nanospheres revealed the anatase diffraction patterns for hollow and porous TiO_2 nanospheres (Supporting Information, Figure S15). The success of producing hollow and porous TiO_2 nanostructures through this strategy not only indicates that we can extend gelatin template to synthesize different metal oxide materials but also presents a potential candidate with high surface area and porosity characteristics for application in photocatalysis.

Conclusions

In summary, we successfully prepared superparamagnetic hollow and paramagnetic porous Gd_2O_3 nanospheres with average sizes below 200 nm, a very attractive T_1 relaxation rate at a low Gd concentration, and low toxicity. We discovered the superparamagnetic property of hollow Gd_2O_3 nanospheres because of their carbon coating. We suggest that it will be beneficial to combine MR imaging with photothermal therapy in the near-infrared region, as suggested in a recent report[32] on FeCo/graphite-shell nanocrystals. Both the porous and hollow Gd_2O_3 nanospheres are promising for encapsulate drugs for controlled release during magnetic delivery. In addition, we have also demonstrated the preparation of hollow and porous TiO_2 nanospheres using gelatin templates. Overall, multifunctional gelatin templates are attractive for developing various hollow and porous metal oxides, or other materials, using the sol−gel process and precursor deposition.

Acknowledgment. This work was supported by the National Science Council, Taiwan. We thank Prof. Hong-Ping Lin for valuable help with the TGA and BET instruments.

Supporting Information Available: Figures S1−S15 (PDF). This material is available free of charge via the Internet at http://pubs.acs.org.

CM703195U

(32) Seo, W. S.; Lee, J. H.; Sun, X.; Suzuki, Y.; Mann, D.; Liu, Z.; Terashima, M.; Yang, P. C.; Mcconnell, M. V.; Nishimura, D. G.; Dai, H. *Nat. Mater.* **2006**, *5*, 971.